Stable all-optical limiting in nonlinear periodic structures. III. Nonsolitonic pulse propagation

Winnie N. Ye, Lukasz Brzozowski, and Edward H. Sargent

Department of Electrical and Computer Engineering, University of Toronto, 10 King's College Road, Toronto, Ontario, Canada M5S 3G4

Dmitry Pelinovsky

Department of Mathematics, McMaster University, 1280 Main Street West, Hamilton, Ontario, Canada L8S 4K1

We present a detailed time-domain analysis of a promising nonlinear optical device consisting of alternating layers of nonlinear materials with oppositely signed Kerr coefficients. We study propagation of nonsolitonic (Gaussian) pulses through the device, whose transmittance characteristics point to potential uses in all-optical switches and limiters. If the optical structure has no linear built-in grating, the pulse experiences a nonsolitonic (amplitude-decaying) propagation in the structure, which exhibits limiting properties depending on the bandwidth of the pulse. We elucidate the conditions under which double imaging occurs within the dynamically formed grating under the pulse propagation. In the presence of the linear out-of-phase grating, we observe strong envelope compression and reshaping of a Gaussian pulse, resulting in stable high-amplitude, multiple-peak oscillations as it propagates through the nonlinear optical structure. © 2003 Optical Society of America

OCIS codes: 230.4320, 190.4360, 230.1480, 190.5530, 200.4740, 230.1150, 190.7110, 200.4740.

1. INTRODUCTION

Today's fiber-optic networks are constrained by the information processing rate of electronics. Efficient optical signal processing devices with picosecond response times would help alleviate this bottleneck. Nonlinear periodic structures represent one class of devices that enable all-optical signal processing.[1–8] These structures have been theoretically predicted and experimentally demonstrated to give rise to all-optical switching,[3,6,9] pulse compression,[4,5] limiting,[7,8,10–13] and logic operations.[3,8]

Recent studies of pulse propagation in nonlinear Bragg gratings have concentrated on Bragg solitons, which arise from the balancing of dispersion of the grating and self-phase modulation due to Kerr nonlinearity. Nonlinear coupled-mode equations predict Bragg solitons, solitary waves that propagate through a grating without changing their shapes. Gap solitons represent the most-studied class of Bragg solitons, with pulse spectra lying entirely within a photonic bandgap.[1,2] The term gap soliton was first introduced in 1987 by Chen and Mills[14]; then Mills and Trullinger[15] proved the existence of gap solitons by analytic methods. Later Sipe and Winful[16] and de Sterke and Sipe[17] showed that the electric field satisfies a nonlinear Schrödinger equation that allows soliton solutions with carrier frequencies close to the edge of the stop band. Christodoulides and Joseph[18] and Aceves and Wabnitz[19] obtained soliton solutions with carrier frequencies close to the Bragg resonance.

Experimental demonstrations of gap solitons have been on soliton propagation, switching, and pulse compression.

Sankey *et al.*[6] reported the first observation of all-optical switching in a nonlinear periodic structure—a corrugated silicon-on-insulator waveguide. Soon after, Herbert *et al.*[7] observed optical power limiting and switching in a three-dimensional colloidal microsphere immersed in a Kerr medium. In 1996 Eggleton *et al.*[2] reported direct observation of soliton propagation and pulse compression in uniform fiber gratings, verifying experimentally for the first time the theories put forth by Christodoulides and Joseph[18] and Aceves and Wabnitz.[19] Pulse compression was also later observed in nonuniform Bragg gratings by Broderick *et al.*[5] Optical pulse compression is attributed to two mechanisms: optical pushbroom and cross-phase modulation. The optical pushbroom effect requires a strong optical pump to alter the local refractive index and thus detune a weak probe pulse from the center of the bandgap, modifying the transmission of the probe.[4] The pump-induced nonlinear index change creates a frequency shift at the trailing edge of the probe pulse. The consequent velocity increase of the trailing edge sweeps the probe energy to the front of the probe pulse, resulting in pulse compression. In contrast, the cross-phase modulation effect works in reflection instead of transmission.[5] This approach facilitates easier observation of the compressed signal since the probe is spatially separated from the pump.

Other than gap-soliton propagation, nonsolitonic pulse propagation has also attracted considerable attention. Instead of maintaining constant pulse shape as with gap solitons, propagation of ultrashort, nonsolitonic pulses in

a device with alternating layers of oppositely signed Kerr materials involves variations in pulse amplitude and shape. When a pulse is launched at the front end of such structure as an incident (forward) wave, the reflected (backward) wave is zero identically. Once the pulse moves through the device, the backward-propagating wave is generated by means of Bragg resonance coupling. Since the reflected wave is always zero at the front of the pulse propagation, the pulse in the incident wave does not trap gap solitons, and so displays nonsolitonlike behavior. Nevertheless we show that pulse propagation behavior depends on the system through which the pulse travels. If the system supports gap-soliton propagation, a nonsolitonic pulse experiences strong compression and pulse reshaping, resulting in high-amplitude-multiple-peak oscillations. If the system does not allow the existence of gap solitons, the amplitude of the pulse decays as it propagates because of reflection into the backward wave.

Gap solitons are certainly of great interest for applications in telecommunications. But the strict requirements of peak power, pulse shape, and duration in producing a soliton to perfectly balance dispersion and nonlinear effect are sometimes hard to satisfy. In contrast nonsolitonic pulses have much more flexibility and the nonsolitonic character allows for self-processing, self-reshaping, and analog functions such as limiting.

We present in this paper the propagation dynamics of nonsolitonic pulses in an optical device with alternating layers of nonlinear materials with oppositely signed Kerr coefficients. The coupled-mode system was derived and evaluated in the steady-state analysis (continuous-wave case) by Pelinovsky *et al.*[10] Optical limiting behavior that allows transmission of only low-intensity radiation was considered in their analysis, with applications in optical switches and hardlimiters. The all-optical limiting was shown to be stable, even under small time-dependent perturbations developed in the nonlinear periodic structure.[10] A numerical method based on finite differences was developed by Pelinovsky *et al.*[11] for which stable transmission of continuous waves was observed in devices with oppositely-signed Kerr coefficients. Recently we have performed time-domain simulations of ultrashort pulse propagation in devices with no linear built-in grating.[12] In the current study, we explore the influence of device length and strength of the linear grating on the behavior of pulse propagation. We also show the limiting behavior of the pulse energy transmittance as a function of the pulse bandwidth, as well as the double imaging of pulses inside the grating. Pulse limiting, reshaping, and compression are observed and studied.

The paper is organized as follows. In Section 2 we describe the coupled-mode equations for nonlinear periodic structures, identify the boundary conditions, define the incident pulse as a Gaussian pulse, and state the balance equations. In Section 3 we derive the exact solutions for gap solitons in the coupled-mode equations and illustrate the nonsolitonic propagation of the Gaussian pulse in the nonlinear periodic structure. In Section 4 we define and justify the material parameters chosen for the numerical simulations. In Section 5 we present analysis of the simulation results and discuss mechanisms behind the observations. Section 6 concludes the paper.

2. MODEL

We adopt coupled-mode equations that describe the resonant Bragg interaction between two counterpropagating waves in the nonlinear periodic structure[10]:

$$i\left(\frac{\partial A_+}{\partial Z} + \frac{\partial A_+}{\partial T}\right) + n_{0k}A_- + n_{nl}(|A_+|^2 + 2|A_-|^2)A_+$$

$$+ n_{2k}[(2|A_+|^2 + |A_-|^2)A_- + A_+^2\bar{A}_-] = 0, \quad (1)$$

$$-i\left(\frac{\partial A_-}{\partial Z} - \frac{\partial A_-}{\partial T}\right) + n_{0k}A_+ + n_{nl}(2|A_+|^2 + |A_-|^2)A_-$$

$$+ n_{2k}[(|A_+|^2 + 2|A_-|^2)A_+ + A_-^2\bar{A}_+] = 0. \quad (2)$$

A_+ and A_- are slowly varying envelope amplitudes of the right-propagating and left-propagating waves, respectively. Parameters n_{ln}, n_{0k}, n_{nl}, and n_{2k} are related to the linear refractive index and Kerr coefficients of the two optical materials that make up the nonlinear periodic grating as follows[10]:

$$n_{ln} = \frac{n_{01} + n_{02}}{2}, \qquad n_{nl} = \frac{n_{nl1} + n_{nl2}}{2},$$

$$n_{0k} = \frac{n_{01} - n_{02}}{\pi}, \qquad n_{2k} = \frac{n_{nl1} - n_{nl2}}{\pi}. \quad (3)$$

The spatial coordinate Z and the evolution time T are normalized as follows: $Z = \omega_0 z/c$ and $T = \omega_0 t/|n_{ln}|$, where ω_0 is the frequency of the Bragg resonance, z and t are physical space and time variables, and c is the speed of light. The period Λ of the nonlinear grating is included in the resonant frequency $\omega_0 = \pi c/(|n_{ln}|\Lambda)$ such that it no longer appears explicitly in the coupled-mode system (1)–(2). The total length of the structure in normalized units is L and the ends of the structure are located at $Z = 0$ and $Z = L$.

Let us consider the nonlinear periodic structure that is built from two optical materials with alternating oppositely-signed Kerr coefficients when $n_{nl1} = -n_{nl2}$ and $n_{nl} = 0$. Under these conditions, the device operates in a true-optical limiting regime for transmission of light waves of constant intensity.[10] In this regime, the pulse transmission is stable even with time-dependent perturbations.[12]

We assume that a pulse is launched into the structure from the left end:

$$I_{in}(T) = |A_+(Z = 0, T)|^2, \qquad I_{ref}(T) = |A_-(Z = 0, T)|^2,$$

$$I_{out}(T) = |A_+(Z = L, T)|^2, \qquad |A_-(Z = L, T)|^2 = 0. \quad (4)$$

$I_{ref}(T)$ is the reflected intensity at the input end of the grating (left end) and $I_{out}(T)$ is the transmitted intensity at the output end of the grating (right end). The incident intensity $I_{in}(T)$ is defined by the optical signal launched at the grating, while the reflected and transmitted intensities $I_{ref}(T)$ and $I_{out}(T)$ are generated dynamically in the time-dependent solutions of the coupled-mode system (1)–(2). The boundary conditions defined in Eq. (4) are satisfied at all times. In addition we assume zero initial

conditions: $A_\pm(Z, T = 0) = 0$. We consider that a Gaussian pulse is launched onto the system:

$$I_{\text{in}}(T) = I_{\text{peak}} \exp\left[-\frac{(T - \mu)^2}{2\sigma^2}\right], \qquad (5)$$

where I_{peak} is the maximal intensity of the pulse, μ is the time delay of the pulse, and σ defines the pulse duration as the full width at half maximum, or $FWHM$:

$$FWHM = 2\sigma(2 \ln 2)^{1/2}. \qquad (6)$$

If $\mu \gg FWHM$, the pulse intensities approach zero at $T = 0$ and we neglect the small mismatch between the pulse intensity $I_{\text{in}}(0)$ and the zero initial condition at $T = 0$.

The coupled-mode system (1)–(2) obeys the balance equation

$$\frac{\partial}{\partial T}(|A_+|^2 + |A_-|^2) + \frac{\partial}{\partial Z}(|A_+|^2 - |A_-|^2) = 0. \qquad (7)$$

Integrating over the nonlinear structure, we find a balance between the incident, reflected, and transmitted intensities:

$$\frac{d}{dT}\int_0^L (|A_+|^2 + |A_-|^2)dZ = I_{\text{in}}(T) - I_{\text{ref}}(T) - I_{\text{out}}(T).$$

If the incident pulse is fully transmitted and no light becomes trapped within the grating in the limit $T \to \infty$, the conservation of total power takes place in the form

$$\mathcal{I}_{\text{in}} = \mathcal{I}_{\text{ref}} + \mathcal{I}_{\text{out}}, \qquad (8)$$

where $\mathcal{I}$ denotes the total incident, reflected, or transmitted intensity, e.g., $\mathcal{I}_{\text{in}} = \int_{-\infty}^{\infty} I_{\text{in}}(T)dT$. The balance between the total intensities enables us to compute the input–output transmission characteristic for propagation of the Gaussian pulse [Eq. (5)], i.e., $\mathcal{I}_{\text{out}}/\mathcal{I}_{\text{in}}$.

3. BEHAVIOR OF SOLITONIC AND NONSOLITONIC PULSES

Since the propagation behavior of nonsolitonic pulses depends on whether the system is soliton supportive, we begin by deriving the exact solutions of the coupled-mode system (1)–(2) for gap solitons. We show that the gap solitons exist in the system for $n_{nl} = 0$, $n_{0k} < 0$, and $n_{2k} > 0$, or alternatively for $n_{nl} = 0$, $n_{0k} > 0$, and $n_{2k} < 0$. The parameter n_{2k} can be normalized to be positive without loss of generality. Then we show that the gap soliton propagates with a constant speed even if the nonlinear periodic structure is long, i.e., in the limit of large L. On the other hand, the nonsolitonic pulse [Eq. (5)] either decays or oscillates in amplitude in long periodic structures. In other words, propagation of Gaussian pulses is intrinsically nonsolitonic.

In order to find exact solutions for gap solitons we rewrite the coupled-mode system (1)–(2) in new coordinates as

$$\zeta = \frac{Z - VT}{(1 - V^2)^{1/2}}, \qquad \tau = \frac{T - VZ}{(1 - V^2)^{1/2}},$$

$$A_\pm(Z, T) = (1 \pm V)^{1/2}a_\pm(\zeta, \tau), \qquad (9)$$

in which the system with $n_{nl} = 0$ takes the form

$$i\left(\frac{\partial a_+}{\partial \zeta} + \frac{\partial a_+}{\partial \tau}\right) + n_{0k}a_- + n_{2k}[2(1 + V)|a_+|^2$$
$$+ (1 - V)|a_-|^2]a_- + (1 + V)a_+^2\bar{a}_-] = 0, \qquad (10)$$

$$-i\left(\frac{\partial a_-}{\partial \zeta} - \frac{\partial a_-}{\partial \tau}\right) + n_{0k}a_+ + n_{2k}[((1 + V)|a_+|^2$$
$$+ 2(1 - V)|a_-|^2]a_+ + (1 - V)a_-^2\bar{a}_+] = 0, \qquad (11)$$

Gap solitons are stationary solutions of the coupled-mode system (1)–(2) that move with constant velocity V and have constant detuning frequency Ω. Separating variables in the system (10)–(11), we write these stationary solutions in the form

$$a_+ = [Q(\zeta)]^{1/2}\exp\{i[\phi(\zeta) - \psi(\zeta)] + i\Omega\tau\},$$
$$a_- = [Q(\zeta)]^{1/2}\exp[i\phi(\zeta) + i\Omega\tau]. \qquad (12)$$

The function $Q(\zeta)$ in Eq. (12) is the intensity of the right-propagating and left-propagating waves, i.e., $Q(\zeta) = |a_+|^2(\zeta) = |a_-|^2(\zeta)$, where we use the balance Eq. (7) for $a_\pm(\zeta, \tau)$ with zero boundary conditions in ζ. The functions $[\phi(\zeta) - \psi(\zeta)]$ and $\phi(\zeta)$ in Eq. (12) are the complex phases of the waves, given that $\psi(\zeta)$ represents the phase difference between the complex phases. It follows from Eqs. (10), (11), and (12) that the functions $Q(\zeta)$ and $\psi(\zeta)$ satisfy the system of differential equations

$$\frac{\partial Q}{\partial \zeta} = \frac{\partial H}{\partial \psi} = -2Q \sin \psi (n_{0k} + 2n_{2k}Q), \qquad (13)$$

$$\frac{\partial \psi}{\partial \zeta} = -\frac{\partial H}{\partial Q} = 2\Omega - 2 \cos \psi (n_{0k} + 4n_{2k}Q), \qquad (14)$$

where the $H = H(Q, \psi)$ is a conserved quantity given by

$$H = 2Q(n_{0k} + 2n_{2k}Q)\cos \psi - 2\Omega Q. \qquad (15)$$

We note that solutions of the system (13)–(14) do not depend on the velocity V. The gap soliton solution satisfies the zero boundary conditions at infinity: $Q(\zeta) \to 0$ as $|\zeta| \to \infty$. Such solutions occur for $H = 0$, when $\cos \psi$ can be eliminated from Eq. (15):

$$\cos \psi = \frac{\Omega}{n_{0k} + 2n_{2k}Q}. \qquad (16)$$

The closed-form solution of the system (13)–(14) can then be written as

$$\left(\frac{\partial Q}{\partial \zeta}\right)^2 + U(Q) = 0,$$

$$U(Q) = -4Q^2[(n_{0k} + 2n_{2k}Q)^2 - \Omega^2]. \qquad (17)$$

The system of Eqs. (17) describes the zero energy level of a particle moving in a potential field $U(Q)$. The critical point $Q = 0$ is a saddle point if $U''(0) < 0$, which necessitates $|\Omega| < |n_{0k}|$. Under this constraint, the trajectory of the solution $Q = Q(\zeta)$ starts from $Q = 0$ in the limit $\zeta = -\infty$, grows exponentially until the turning point $Q = Q_{\text{sol}}$, where $U(Q_{\text{sol}}) = 0$, and then decays exponen-
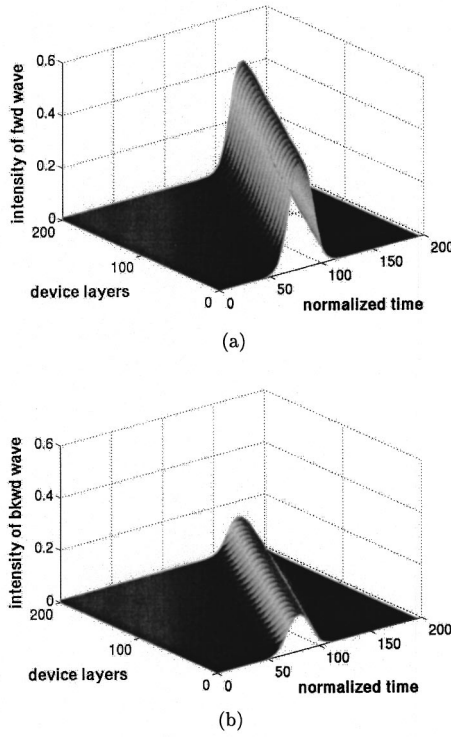
Fig. 1.   Bragg soliton propagation in the system (1)–(2) with $n_{nl} = 0$, $n_{0k} = -0.1$, $n_{2k} = 1/2\pi \times 10^{-12}$ cm^2/W.   Shown are (a) intensity of the forward wave and (b) intensity of the backward wave.   Parameters of the Bragg soliton are $V = 0.5$, $\Omega = 0.01$.

tially to $Q = 0$ in the limit $\zeta \to +\infty$.   If $n_{2k} > 0$ and $n_{0k} < 0$, the turning point exists at

$$Q_{\text{sol}} = \frac{|n_{0k}| - |\Omega|}{2n_{2k}}.$$

The analytical expression for the gap soliton can be derived from Eqs. (17) and is found to take the form

$$Q(\zeta) = \frac{n_{0k}^2 - \Omega^2}{2n_{2k}(|\Omega|\cosh \gamma\zeta + |n_{0k}|)}, \qquad (18)$$

where $\gamma = 2(n_{0k}^2 - \Omega^2)^{1/2}$.   The gap soliton is centered at $\zeta = 0$, where $Q(0) = Q_{\text{sol}}$ and is exponentially localized such that $Q(\zeta) \to Q_\infty \exp(-\gamma|\zeta|)$ as $|\zeta| \to \infty$.

The gap soliton solution [Eq. (18)] exists for $n_{2k} > 0$, $n_{0k} < 0$, and $0 \neq |\Omega| < |n_{0k}|$, i.e., when the nonlinear grating has an out-of-phase, built-in modulation of the linear refractive index.   We use the out-of-phase gratings to refer to the case when the material with the lower linear index has a positive Kerr coefficient and the material with the higher linear index has a negative Kerr coefficient.

We have simulated propagation of a gap soliton in the coupled-mode system (1)–(2) with $n_{nl} = 0$, $n_{2k} = 1/2\pi \times 10^{-12}$ cm^2/W, and $n_{0k} = -0.1$.   Parameters of the gap solitons are $V = 0.5$ and $\Omega = 0.01$.   Propagation of the gap soliton is shown in Fig. 1(a) and 1(b).   They show the intensities of the forward and backward waves $|A_\pm|^2$.   Being injected into the grating initially, the gap soliton propagates with a constant speed V and a constant detuning frequency Ω from the center of the stop-band fre-

quency ω_0.   The envelope amplitudes of both the forward- and backward-propagating waves remain constant spatially.   The steady propagation of gap solitons can be observed in devices of large L.

For comparison, we have also simulated propagation of a Gaussian pulse [Eq. (5)] in the coupled-mode system (1)–(2) with pulse specifications similar to the soliton case ($I_{\text{peak}} = 55$ GW/cm^2 and $FWHM = 27$ fs) and with $n_{nl} = 0$ and $n_{2k} = 1/2\pi \times 10^{-12}$ cm^2/W.   We observe two characteristic scenarios of Gaussian pulse propagation, depending on the parameter n_{0k}.   If $n_{0k} = 0$, the pulse amplitude decays with longer propagation distance and the pulse width grows.   This scenario is shown in Fig. 2.   If $n_{0k} = -0.1$, the pulse amplitude experiences strong compression, pulse reshaping, and high-amplitude multiple-peak oscillations.   This scenario is shown in Fig. 3.   Pulse compression–decompression cycling is observed in the system (1)–(2) in the case when $n_{0k} < 0$, and pulse amplitude decay is observed when $n_{0k} \gtrsim 0$.   Gap soliton propagation is possible in the former case, but is not allowed in the latter case.

In the rest of this section, we prove analytically that pulse compression can be experienced with an out-of-phase, built-in linear grating, assuming the incident pulse takes the form of [Eq. (5)].   For $n_{nl} = 0$, zero initial conditions, and a real boundary value of $A_+(0, T) = [I_{\text{in}}(T)]^{1/2}$, the coupled-mode system (1)–(2) can be simplified to

$$A_+ = u(Z, T), \qquad A_- = iy(Z, T),$$

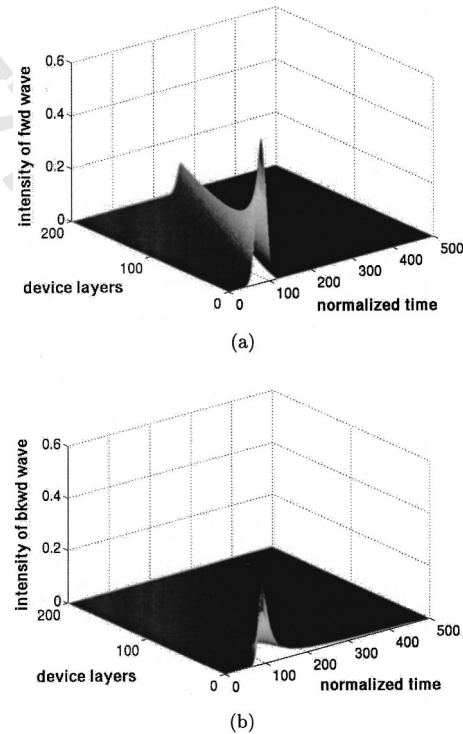where u and y are real variables satisfying the system

Fig. 2.   Decaying Gaussian pulse propagation in the system (1)–(2) without built-in linear grating: $n_{nl} = 0$, $n_{0k} = 0$, $n_{2k} = 1/2\pi \times 10^{-12}$ cm^2/W.   Shown are (a) intensity of the forward wave and (b) intensity of the backward wave.   Parameters of the Gaussian pulse are $I_{\text{peak}} = 55$ GW/cm^2, $FWHM = 27$ fs.
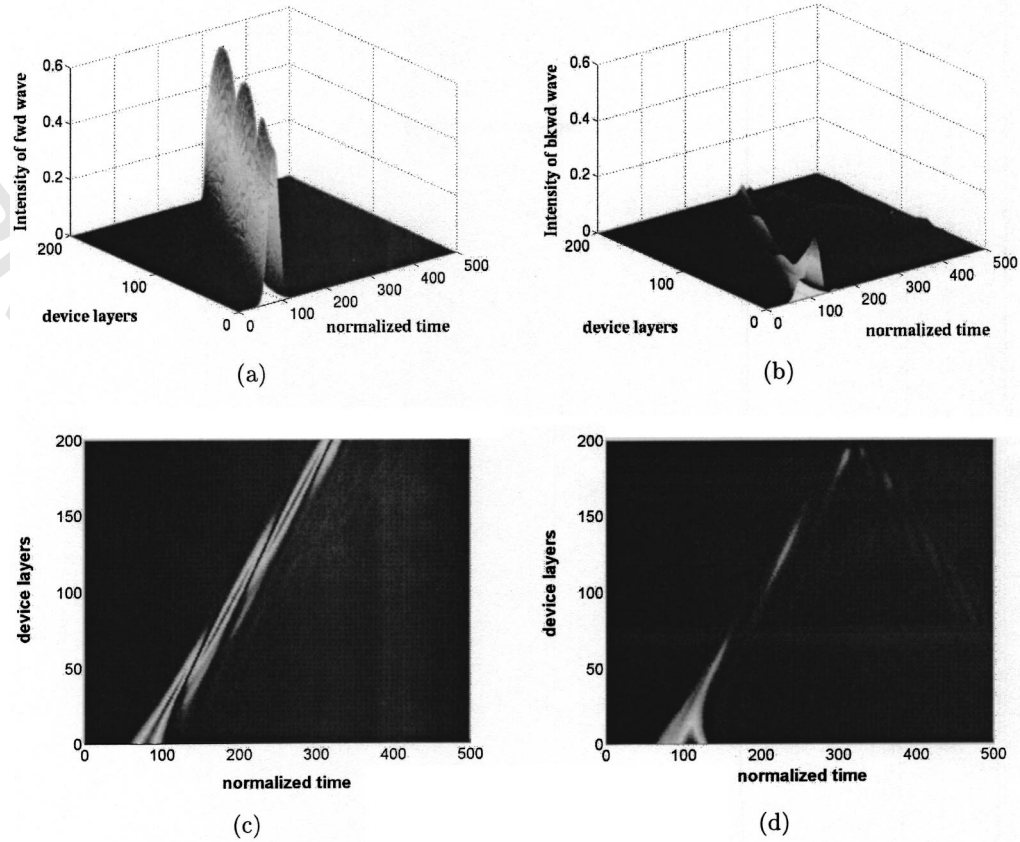
Fig. 3.   Propagation of a launched Gaussian pulse in the system with out-of-phase, built-in linear grating $n_{0k} = -0.1$; compression–decompression cycling is observed.   The other parameters are the same as in Fig. 2.   Shown are (a) intensity of the forward wave; (b) intensity of the backward wave; (c) top view of the three-dimensional graph of panel (a); (d) top view of the graph of panel (b).

$$\frac{\partial u}{\partial Z} + \frac{\partial u}{\partial T} = -[n_{0k} + n_{2k}(u^2 + y^2)]y, \tag{19}$$

$$\frac{\partial y}{\partial Z} - \frac{\partial y}{\partial T} = -[n_{0k} + n_{2k}(u^2 + y^2)]u. \tag{20}$$

It follows from Eq. (20) with $n_{0k} < 0$ that the time derivative $\partial y/\partial T$ is negative for $y \approx 0$ and $0 < u(T) < (I_{cl})^{1/2}$. Here $I_{cl} = |n_{0k}|/n_{2k}$ is the closing intensity. Therefore when the Gaussian pulse [Eq. (5)] enters the device at the input $Z = 0$, the generated backward wave field y is always negative. The other Eq. (19) defines the rate of change of the pulse amplitude in the reference frame moving to the right with unit speed (the speed of the Gaussian pulse). At the peak of the Gaussian pulse, the rate of change is positive if $y < 0$ and $I_{peak} > I_{cl}$. Therefore the Gaussian pulse with the peak intensity I_{peak} exceeding the closing intensity I_{cl} is compressed in width and increased in peak amplitude by the out-of-phase, built-in linear grating. On the other hand, similar analysis shows that the Gaussian pulse with $I_{peak} < I_{cl}$, or the Gaussian pulse in the in-phase, built-in linear gratings with $n_{0k} \geq 0$, is decompressed in width and decreased in amplitude during propagation in the nonlinear periodic structure.

To summarize, when a gap soliton [Eq. (12)] is launched at the input of the optical device, it propagates throughout the periodic structures as a uniformly shaped soliton pulse in both coupled counterpropagating waves. When a Gaussian pulse [Eq. (5)] is launched at the input of the optical device, it propagates as a forward wave, generates a reflected backward wave, and displays nonsoliton behavior: Pulse amplitude decays or pulse compresses, reshapes, and oscillates.

4.   MATERIAL PARAMETERS

Here we discuss the physical approximations behind the derivation of the coupled-mode system (1)–(2). We also describe the choice of material parameters n_{0k} and n_{2k} in numerical modeling of the system, based on device applications.

In the derivation of the coupled-mode system (1)–(2), we have assumed that the response time of the optical material is much smaller than the duration of the pulse envelope. In the present work, we typically assume a maximum index change of 0.01. Experimentally, refractive index changes as large as 0.1 have been obtained. Ultrafast index changes have been reported in systems such as polymers doped with azobenzenes, low-temperature-grown GaAs, or helium-plasma-assisted molecular-beam-epitaxy InGaAsP.[20–23] The response time of the materials was reported to be as fast as 2 ps.[21,22]

In deriving the system (1)–(2), we have also neglected the effects of absorption. In reality, materials which exhibit ultrafast index changes as large as 0.1 have signifi-
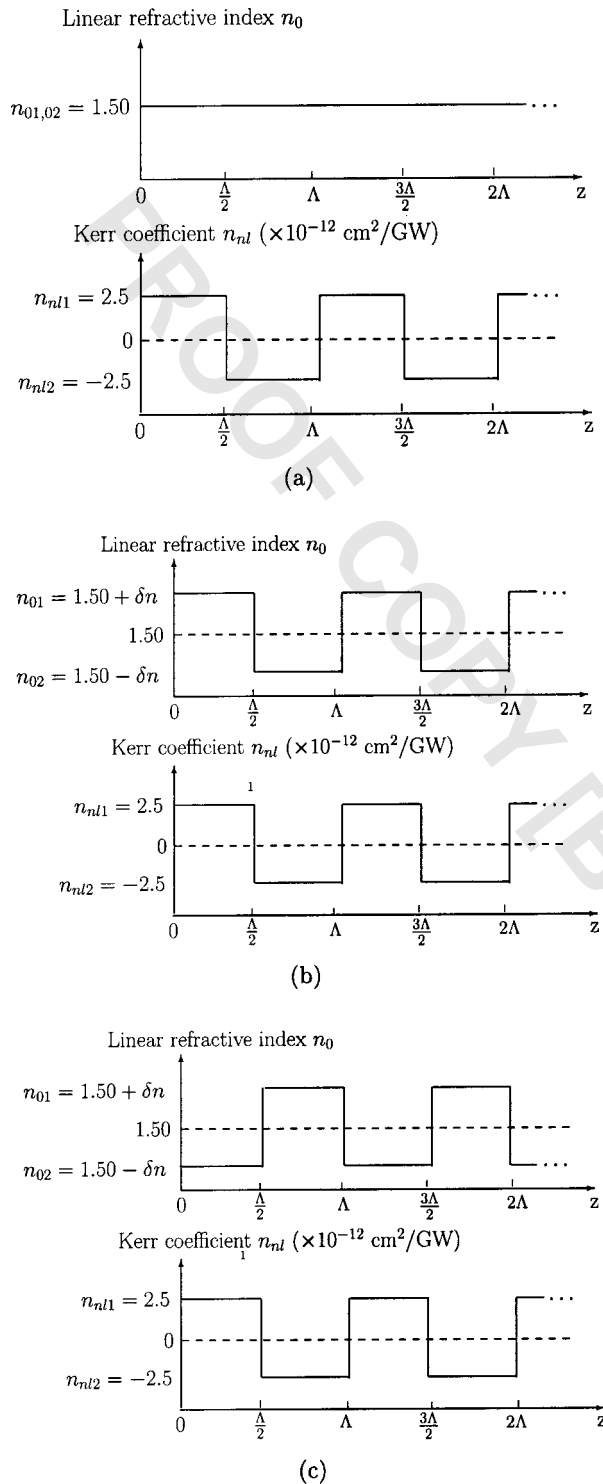
Fig. 4. Nonlinear periodic device consists of alternating layers of nonlinear materials with oppositely-signed Kerr coefficients. The refractive indices of two adjacent layers are $n_{01} + n_{nl1}I$ and $n_{02} + n_{nl2}I$. We study three cases: (a) no linear grating; (b) in-phase, linear, built-in grating; (c) out-of-phase, linear, built-in grating.

cant linear absorption. To illustrate, devices made from such highly nonlinear materials would need to be at least 2 μm thick to give rise to the class of transfer functions considered herein. Over such length a device would lose up to 50% of the transmitted power as a result of absorp-

tion. This effect would limit the performance of the optical device. It was previously shown that the omission of some nonlinear effects (such as saturation of nonlinearity) can lead to incorrect prediction of very-high-intensity behavior.[24] Since in the analysis reported herein, we do not include the absorption and saturation effects, exact results of some computations, such as closing intensity, constant transmittance occurring at high incident intensity, or degree of pulse compression could be significantly altered. However the qualitative behavior of the most important trends (e.g., transfer function shape) should be correct.[9] We also note that index changes of 0.01 can be obtained at spectral points at which the absorption and saturation effects are lower by orders of magnitude.[25]

Throughout the simulations the Kerr coefficients $n_{nl1,2}$ of the two adjacent layers are $n_{nl1} = -n_{nl2} = 2.5 \times 10^{-12}$ cm^2/W, and the average linear index is fixed at $n_{ln} = 1.50$. The center frequency of the incident pulse is fixed at $f_0 = 2 \times 10^{14}$ Hz (or at wavelength $\lambda_0 = 1.50$ μm). This choice gives the values $n_{nl} = 0$ and $n_{2k} = 1/2\pi \times 10^{-12}$ cm^2/W in the coupled-mode system (1)–(2).

We analyze propagation of a Gaussian pulse [Eq. (5)] through the periodic optical device for three different cases (as shown in Fig. 4): (A) no linear built-in grating, $n_{0k} = 0$, (B) in-phase, built-in grating, $n_{0k} > 0$, and (C) out-of-phase grating, $n_{0k} < 0$.

5. NUMERICAL SIMULATIONS OF GAUSSIAN PULSE PROPAGATION

A. Case I: $n_{0k} = 0$
The steady state behavior of this device in Fig. 5 shows the energy transmittance as a function of incident pulse intensity. The energy transmittance is defined as the ratio of total pulse transmitted intensity $\mathcal{I}_{\text{out}}$ to the total pulse incident intensity $\mathcal{I}_{\text{in}}$, where the total intensities are defined in Eq. (8). The inset of Fig. 5 illustrates the limiting behavior, in which the intensity of the transmit-
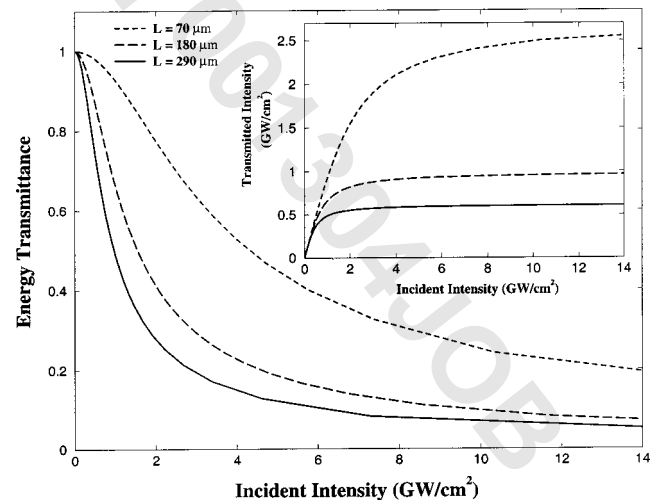

Fig. 5. Steady state analysis: transmittance as a function of incident intensity level for various device lengths: $L = 70$ μm, 180 μm and 290 μm. Inset: transmitted intensity level versus incident intensity for the same device, demonstrating characteristic limiting behavior.

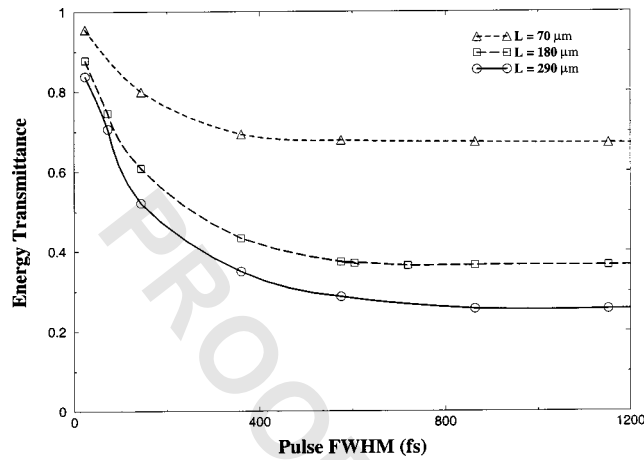Fig. 6. Pulse transmittance as a function of pulse width for a fixed peak pulse intensity of $I_{peak} = 4$ GW/cm^2. The transmittance of the device with length $L = 70$ μm, 180 μm, and 290 μm drops to a limiting value.
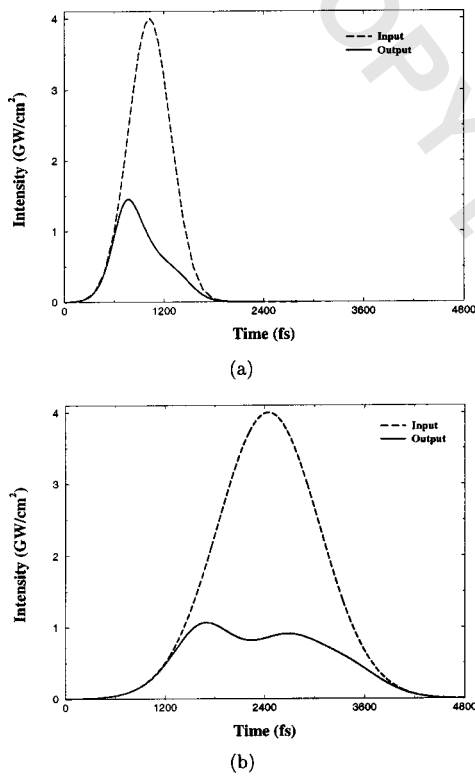

Fig. 7. Input and output intensities of pulse through a 180-μm-long device for an input pulse width of (a) 605 fs or characteristic length of 180 μm, and (b) 1440 fs or characteristic length of 435 μm.

ted light is clamped and approaches asymptotically the limiting intensity for increasing incident intensity.

The energy transmittance of the pulses is shown as a function of pulse width in Fig. 6. In these numerical computations, the incident pulse takes the form of Eq. (5) with a peak pulse intensity chosen to be $I_{peak} = 4$ GW/cm^2, such that the maximum magnitude of change in the refractive index is 0.01. The graph shows that the limiting behavior of the pulse transmission depends on its bandwidth (see also in Ye *et al.*[12]). The long-

duration pulses in Fig. 6 exhibit the desired limiting behavior because their spectral bandwidth lies entirely inside the stop band of the grating, leading to bandwidth-independent transmittance. Short-duration pulses, on the other hand, have a spectral bandwidth which exceeds the width of the dynamic stop band, resulting in transmission of the portion of the power which lies outside the stop band of the device. The knee in the characteristic of Fig. 6 occurs when the pulse bandwidth and nonlinear filter bandwidth become comparable:

$$\omega_{filter} = \frac{4(n_{nl1} - n_{nl2})I_{peak}}{\pi(n_{01} - n_{02})}\omega_0. \tag{21}$$

In Fig. 6 the transmittance decreases from 0.75 to 0.25 when the device length is increased from 70 μm to 290 μm, because stationary gap solitons are not transmitted through the periodic structure with constant linear refractive index. The pulse intensity decays along the device length during the pulse transmission.

Because the Gaussian pulse propagation has a nonsoliton character, the pulse amplitude decays as it propagates in the nonlinear structure. Not only is the amplitude affected, but the shape of Gaussian pulses is also strongly distorted, depending on the size of the structure and ini-
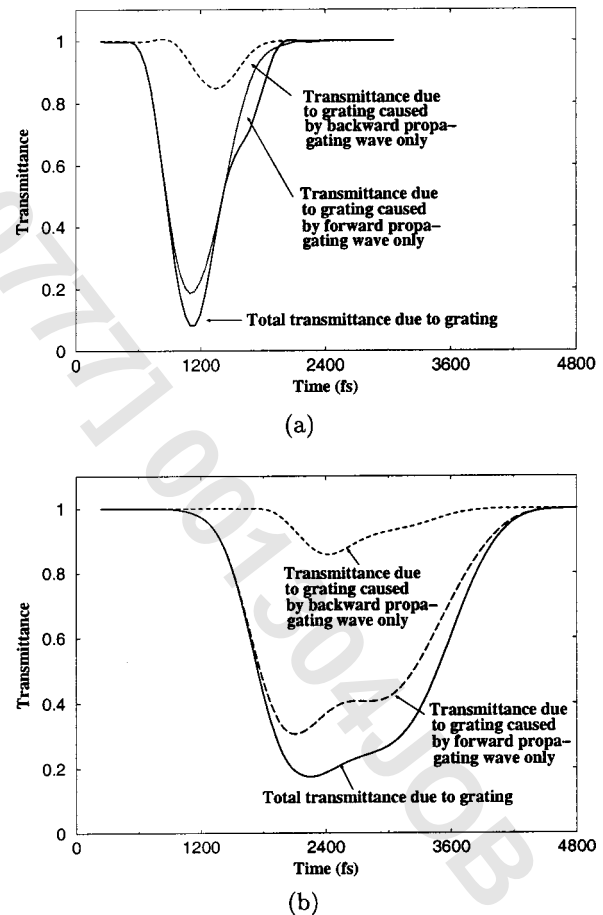

Fig. 8. Heuristic analysis of pulse shaping in a 180-μm-long nonlinear grating. The time-dependent, instantaneous transmittance is attributable to contributions from the forward- and backward-propagating pulse for an input pulse width of (a) 605 fs or characteristic length of 180 μm, and (b) 1440 fs or characteristic length of 435 μm.
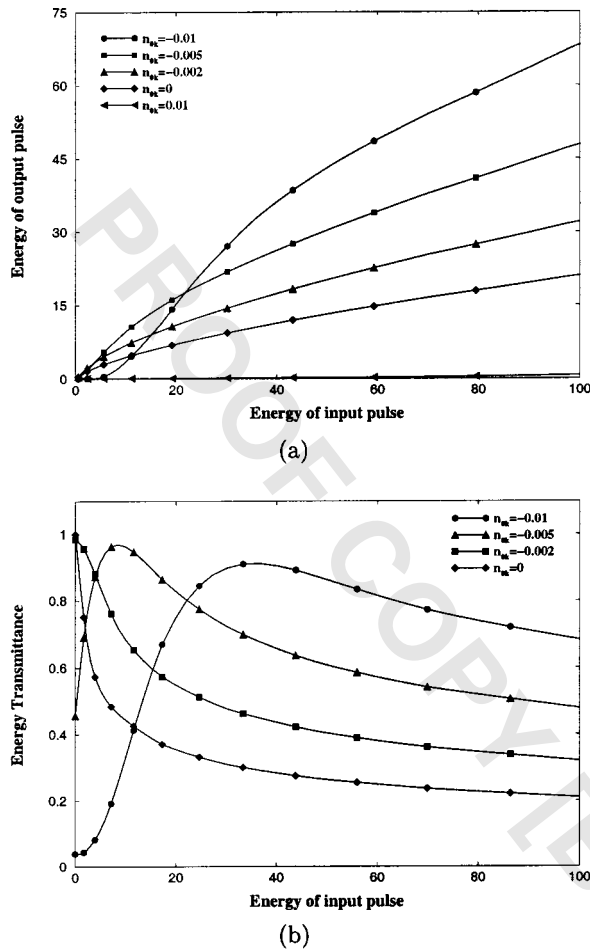
Fig. 9.   (a) Total pulse transmitted intensity versus total pulse incident intensity; (b) corresponding energy transmittance as a function of pulse energy incident for linear in- and out-of-phase built-in gratings.   Pulse width of 605 fs and device length of 180 μm were fixed for all cases.

tial pulse width.   We show in Fig. 7(a) and 7(b) the transmitted pulse shapes through a 180-μm-long device for two different temporal widths.

The bandwidth of both pulses is much less than the effective bandwidth of the device, allowing us to focus attention on intensity self-patterning of the pulses by removing the effects of incomplete spectral blocking.   To explain the distortion in transmitted pulses, we calculate the time-dependent transmittance of the induced nonlinear grating, as illustrated in Fig. 8(a) and 8(b).   For the shorter pulse length of 180 μm, Fig. 8(a) shows that the forward- and backward-propagating waves form their strongest instantaneous gratings at different times.   The backward-propagating wave gives rise to an additional delayed replica of the transmitted pulse in the time-dependent transmittance, causing a dip in the transmitted pulse of Fig. 7(a).   When the incident pulse is longer than the device (435 μm in this example), the strongest instantaneous gratings are formed roughly at the same time period for forward- and backward-propagating waves [Fig. 8(b)].   Sequential multiple reflections of pulses inside the relatively short structure create echoed patterning of the transmitted pulse, as seen in Fig. 7(b).

B. Case II: $n_{0k} > 0$

We now consider periodic structures with an in-phase, linear, built-in grating, with $n_{0k} > 0$ and $n_{2k} > 0$.   The intensity-induced nonlinear grating adds constructively to the existing built-in linear grating, resulting in low transmittance.   No significant transmitted pulse energy is observed for a large range of different input pulses, because most of the incident light is blocked by the linear built-in grating.   This is evident in the bottom curve of Fig. 9(a), constructed for the in-phase linear grating with $n_{0k} = 0.01$.

C. Case III: $n_{0k} < 0$

Here we consider periodic structures with an out-of-phase, linear, built-in grating, with $n_{0k} < 0$ and $n_{2k} > 0$.   Such a grating allows for a dynamic balance to the intensity-induced nonlinear grating as the pulse propagates through the structure.   In other words, the grating is gradually bleached then regained as the incident pulse propagates through the structure.

We first investigate the effects of grating strength on the transmittance of the device.   In this analysis, a fixed incident pulse width of 605 fs is launched at structures with linear out-of-phase gratings of $n_{0k} = -0.002$, $n_{0k} = -0.005$, and $n_{0k} = -0.01$.   The intensity $I_{\text{cl}} = |n_{0k}|/n_{2k}$ that causes the nonlinear index change to balance completely with the out-of-phase linear grating is referred to as the closing intensity, as noted in Section 3.   When the balance between linear and nonlinear grating closes the overall grating profile, the device is locally transparent.   The total pulse transmitted intensity versus the total pulse incident intensity is shown in Fig. 9(a) for the out-of-phase linear gratings listed above.   The pulse energy transmittance is shown in Fig. 9(b) for the same out-of-phase linear gratings.

When the out-of-phase linear grating is large enough to effect a significant built-in reflectance for the device (for example, when the built-in linear index difference is 0.01), the transmittance reveals an interplay between built-in and intensity-dependent grating behavior.   At small incident pulse intensities the linear built-in grating
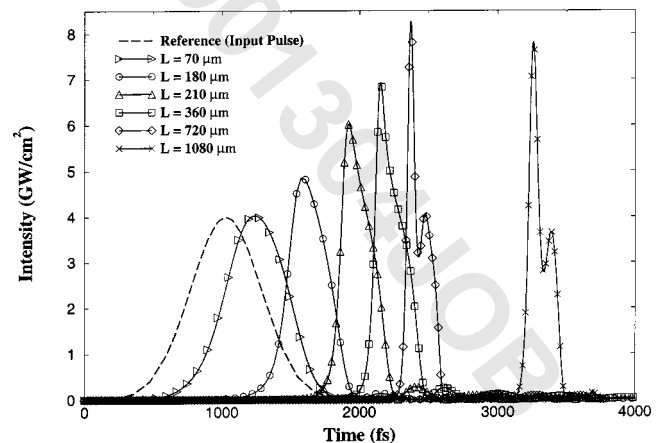

Fig. 10.   Output temporal response of the device with length L = 70 μm, 180 μm, 290 μm, 360 μm, 720 μm, and 1080 μm for a fixed input pulse with $I_{\text{peak}} = 4$ GW/cm^2 and $FWHM = 605$ fs.   Pulse compression, reshaping, and double-peak oscillations are observed.
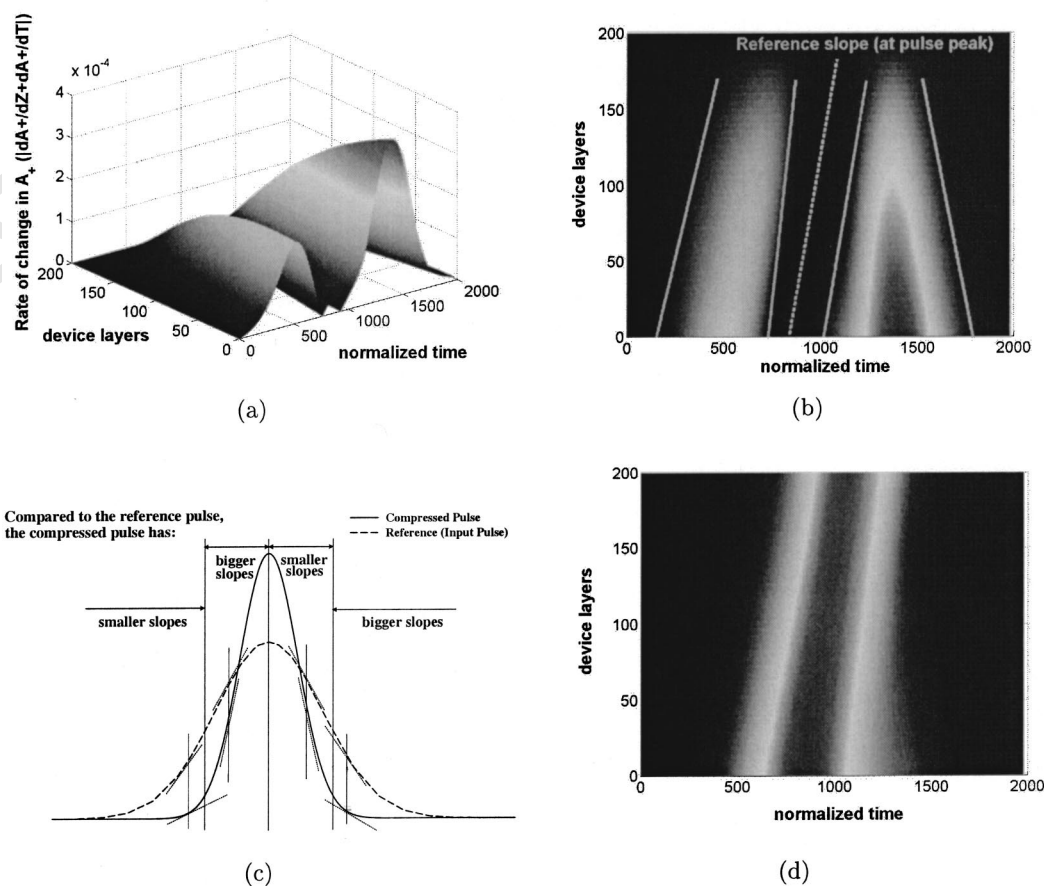
(a)

(b)

(c)

(d)

Fig. 11. (a) Rate of change in amplitude of the forward-propagating wave; (b) top view of (a); (c) a simplified two-dimensional diagram of a Gaussian incident pulse and a compressed pulse; (d) top view of the intensity profile with respect to time and space. An incident pulse with $I_{\text{peak}} = 4$ GW/cm^2, $FWHM = 605$ fs is launched at the input of a 180-μm-long device.

blocks most of the light, resulting in a transmittance close to 0. The transmittance gradually increases as the increasing intensity-induced nonlinear index change offsets the linear grating. The closing and the reopening of the grating are responsible for the S-curve character of the transfer function in Fig. 9(a) which may be used for optical logic gates such as an OR gate.[8,13] The energy transmittance is at its maximum when the peak intensity of the incident pulse is at the closing intensity and the regions around the peak of the pulse bleach out the grating.

Long-duration pulses exhibit the limiting trend of Fig. 9(b). However the energy transmittance of small linear, built-in gratings does not converge to the transmittance of gratings without a linear index change: The more intense are the input pulses, the more there exist regions where the self-induced nonlinear grating matches with the built-in linear grating, and the transmittance is higher than that with no linear grating.

We proceed to examine the influence of device length on transmitted pulse shapes in the presence of the out-of-phase linear grating with $n_{0k} = -0.01$. We fix the peak intensity of the incident pulse at a value of $I_{\text{peak}} = 4$ GW/cm^2 to close the grating and the pulse width at $FWHM = 605$ fs. All stages of the pulse compression, reshaping, and high-amplitude, multiple-peak oscillations are shown in Fig. 10 for different device lengths. This process resembles the Gaussian pulse propagation in

the out-of-phase linear gratings displayed in Fig. 3. Figure 3 and Fig. 10 differ only in the parameters used for the incident pulse. For smaller peak intensity I_{peak} and larger pulse width $FWHM$, the pulse reshaping and multiple-peak oscillations in Fig. 10 occur at distances $L > 300$ μm, much larger compared with those in Fig. 3. The initial stage of pulse compression occurs at distances $L < 300$ μm, when the compressing Gaussian pulse preserves a single-peak structure.

To validate and explain the observation of pulse compression, we seek to reveal the development of the pulse, and consequently the instantaneous grating, in time and space across the device. We show in Fig. 11(a) and 11(b) the rate of change of the amplitude of the forward-propagating wave ($\partial A_+/\partial T + \partial A_+/\partial Z$) in a 180-$\mu$m-long device. As follows from Eq. (19), the forward-propagating wave is enhanced when the backward-propagating wave is coupled in. Moreover the rate of change of amplitude $A_+(Z, T)$ resembles the profile of the backward-propagating envelope $A_-(Z, T)$. The M-shaped graph along the time axis in Fig. 11(a) describes the existence of a pulse propagating along the device length.

Figure 11(b) provides physical evidence of pulse compression. In Fig. 11(c) we compare a Gaussian pulse to a compressed pulse. The slope of the amplitude of the envelope decreases at the beginning stage of the focusing
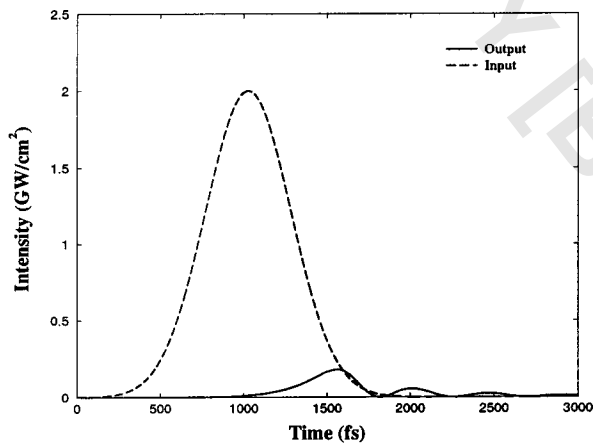
process. The slope then increases drastically before reaching the peak. Similar arguments apply to the second half of the compressed pulse, except the slope decreases after the peak and increases at the final stages of the focusing process. The convergence of the four slopes of the M-shape along the device length in Fig. 11(b) demonstrates the changes in slopes associated with compression.

As the pulse propagates through the structure, the intensity-induced nonlinear grating gradually closes the total grating. The sum of forward- and backward-propagating intensities can give rise to an instantaneous peak intensity which exceeds that required to close the grating completely at some time instances. For a short period of time the nonlinear grating dominates the index grating, which creates a slight in-phase total grating (positive values). Figure 11(d) depicts this process in a 500-layer (180-μm-long) device. The front of the pulse travels approximately at the same speed as the peak of the pulse. The trailing edge, however, catches up with the leading edge, resulting in pulse compression. The effect brings to mind a pushbroom, as described by Broderick *et al.*[4,5] Instead of using both pump signal and probe
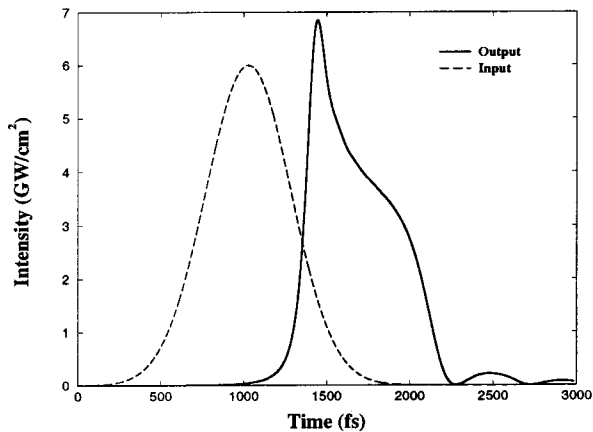
beam, we use only one strong pulse to alter the local refractive index of the medium, resulting in a self-pushbroom.

The compression effects are observed when the peak pulse intensity I_{peak} is set to close completely the grating, i.e., $I_{\text{peak}} = I_{\text{cl}} = |n_{0k}|/n_{2k}$. If the intensity-induced nonlinear grating is small compared to the out-of-phase linear grating, the transmittance is expected to be lower due to reflection by the grating. We simulate a pulse [Eq. (5)] with peak intensity $I_{\text{peak}} = 2$ GW/cm^2 which gives a maximum nonlinear grating of 0.005 (lower than the out-of-phase linear grating $n_{0k} = -0.01$). Figure 12(a) shows the low transmittance and decay of the output pulse. In the case of higher input peak intensity I_{peak}, the nonlinear grating will dominate the grating profile, resulting in a sign-switching of the grating profile. Similar to the case $I_{\text{peak}} = 4$ GW/cm^2, the energy of forward- and backward-propagating waves will be stored inside the grating, causing pulse compression during transmission. Figure 12(b) shows the simulated compressed output pulse when the peak incident pulse is $I_{\text{peak}} = 6$ GW/cm^2, corresponding to a maximum induced nonlinear grating of 0.015 (higher than the out-of-phase linear grating $n_{0k} = -0.01$).

Summarizing, we observe envelope compression in the nonlinear optical structures with an out-of-phase, built-in linear grating when the device length does not exceed twice the input pulse width and the peak input intensity matches or exceeds that required to close the grating.

6. CONCLUSION

We have investigated the propagation dynamics of ultrashort pulses in a nonlinear periodic structure with variation of the grating length and linear grating strength. We have studied the pulse behavior for the no-built-in grating, in-phase, built-in grating, and out-of-phase grating cases. In the absence of the linear grating, the energy transmittance of pulses with small bandwidth (compared to the bandwidth of the grating) is independent of pulse width. In other words, the limiting behavior of the device is pulse-bandwidth-dependent. We have distinguished the mechanism behind pulse shape formation for long-duration pulses from that for short-duration pulses. In the presence of the linear grating, S-shaped transmittance characteristics have been observed resulting from expansion and contraction of the stop band. We have described a compression effect reminiscent of the pump-probe pushbroom for a single pulse. The analysis of the temporal pulse propagation presented in this paper explores the potential optical signal processing functions such as limiting, logic gate operation, and pulse reshaping of a novel, nonlinear Bragg structure.

W.N. Ye may be reached by e-mail at winnie.ye @utoronto.ca.

Fig. 12. Output transmitted pulse shapes when the intensity of an incident Gaussian pulse is set to (a) $I_{\text{peak}} = 2$ GW/cm^2 and (b) $I_{\text{peak}} = 6$ GW/cm^2. The width of the pulse is $FWHM = 605$ fs and the device is fixed to $L = 180$ μm.

REFERENCES

1. C. M. de Sterke and J. E. Sipe, "Gap solitons," Prog. Opt. **33**, 203–259 (1994).
2. B. J. Eggleton, R. E. Slusher, C. M. de Sterke, P. A. Krug,

and J. E. Sipe, "Bragg grating solitons," Phys. Rev. Lett. **76**, 1627–1630 (1996).

3. N. G. R. Broderick, D. Taverner, and D. J. Richardson, "Nonlinear switching in fiber Bragg gratings," Opt. Express **3**, 447–453 (1998).

4. N. G. R. Broderick, D. Taverner, D. J. Richardson, M. Ibsen, and R. I. Laming, "Optical pulse compression in fiber Bragg gratings," Phys. Rev. Lett. **79**, 4566–4569 (1997).

5. N. G. R. Broderick, D. Taverner, D. J. Richardson, M. Ibsen, and R. I. Laming, "Experimental observation of nonlinear pulse compression in nonuniform Bragg gratings," Opt. Lett. **22**, 1837–1839 (1997).

6. N. D. Sankey, D. F. Prelewitz, and T. G. Brown, "All-optical switching in a nonlinear periodic-waveguide structure," Appl. Phys. Lett. **60**, 1427–1429 (1992).

7. C. J. Herbert, W. S. Capinsky, and M. S. Malcuit, "Optical power limiting with nonlinear periodic structures," Opt. Lett. **17**, 1037–1039 (1992).

8. L. Brzozowski and E. H. Sargent, "Optical signal processing using nonlinear distributed feedback structures," IEEE J. Quantum Electron. **36**, 550–555 (2000).

9. J. He and M. Cada, "Optical bistability in semiconductor periodic structures," IEEE J. Quantum Electron. **27**, 1182–1188 (1991).

10. D. Pelinovsky, L. Brzozowski, J. Sears, and E. H. Sargent, "Stable all-optical limiting in nonlinear periodic structures. I. Analysis," J. Opt. Soc. Am. B **19**, 43–53 (2002).

11. D. Pelinovsky and E. H. Sargent, "Stable all-optical limiting in nonlinear periodic structures. II. Computations," J. Opt. Soc. Am. B **19**, 1873–1889 (2002).

12. W. N. Ye, L. Brzozowski, E. H. Sargent, and D. Pelinovsky, "Nonlinear propagation of ultrashort pulses in nonlinear periodic materials with oppositely-signed Kerr coefficients," in *IEEE LEOS Annual General Meeting Proceedings* (Institute of Electrical and Electronics Engineers, San Diego, 2001), pp. 441–442.

13. E. Johnson and E. H. Sargent, "Function and sensitivity of signal processing systems using addition followed by limiting," J. Lightwave Technol. (to be published).

14. W. Chen and D. L. Mills, "Gap solitons and the nonlinear optical response of superlattices," Phys. Rev. Lett. **58**, 160–163 (1987).

15. D. L. Mills and S. E. Trullinger, "Gap solitons in nonlinear periodic structures," Phys. Rev. B **36**, 947–952 (1987).

16. J. E. Sipe and H. G. Winful, "Nonlinear Schrödinger solitons in a periodic structure," Opt. Lett. **13**, 132–133 (1988).

17. C. M. de Sterke and J. E. Sipe, "Envelope-function approach for the electrodynamics of nonlinear periodic structures," Phys. Rev. A **38**, 5149–5165 (1988).

18. D. N. Christodoulides and R. I. Joseph, "Slow Bragg solitons in nonlinear periodic structures," Phys. Rev. Lett. **62**, 1746–1749 (1989).

19. A. B. Aceves and S. Wabnitz, "Self-induced transparency solitons in nonlinear refractive periodic media," Phys. Lett. A **141**, 37–42 (1989).

20. R. Rangel-Rojo, S. Yamada, H. Matsuda, and D. Yankelevich, "Large near-resonance third-order nonlinearity in an azobenzene functionalized polymer film," Appl. Phys. Lett. **72**, 1021–1023 (1998).

21. H. S. Loka, S. D. Benjamin, and P. W. E. Smith, "Optical characterization of GaAs for ultrafast switching devices," IEEE J. Quantum Electron. **34**, 1426–1437 (1998).

22. L. Qian, S. D. Benjamin, P. W. E. Smith, B. J. Robinson, and D. A. Thompson, "Picosecond carrier lifetime and large optical nonlinearities in InGaAsP grown by helium-plasma-assisted molecular beam epitaxy," Opt. Lett. **22**, 108–110 (1997).

23. E. Garmire, "Resonant optical nonlinearities in semiconductors," IEEE J. Sel. Top. Quantum Electron. **6**, 1094–1110 (2000).

24. J. D. Begin and M. Cada, "Exact analytic solutions to the non-linear wave equation for a saturable Kerr-like medium: modes of non-linear optical waveguides and couplers," IEEE J. Quantum Electron. **30**, 3006–3016 (1994).

25. A. Underhill, C. Hill, A. Charlton, S. Oliver, and S. Kreshaw, "Third-order NLO properties of PMMA films co-dispersed with metal dithiolene oligomers," Synth. Met. **71**, 1703–1704 (1995).